Computers and Mathematics with Applications 70 (2015) 1659–1675

Contents lists available at ScienceDirect

Computers and Mathematics with Applications

journal homepage: www.elsevier.com/locate/camwa

Isogeometric collocation methods with generalized B-splines

Carla Manni [a], Alessandro Reali [b,c,d,*], Hendrik Speleers [a]

[a] Department of Mathematics, University of Rome "Tor Vergata", Italy
[b] Department of Civil Engineering and Architecture, University of Pavia, Italy
[c] Institute for Advanced Study, Technische Universität München, Germany
[d] IMATI-CNR, Pavia, Italy

ARTICLE INFO

Article history:
Available online 18 April 2015

Keywords:
Isogeometric analysis
Generalized B-splines
Collocation methods

ABSTRACT

We introduce isogeometric collocation methods based on generalized B-splines and we analyze their performance through numerical examples for univariate and multivariate scalar- and vector-valued problems. In particular, advection–diffusion and linear elasticity model problems are addressed. The resulting method combines the favorable properties of isogeometric collocation and the geometrical and analytical problem-oriented advantages of generalized B-splines.

1. Introduction

Introduced nearly a decade ago in a seminal paper by Hughes et al. [1], isogeometric analysis (IgA) is now a well-established paradigm for the analysis of problems governed by partial differential equations (PDEs), see, e.g., [2] and references therein. It aims at improving the connection between numerical simulation and computer aided design (CAD) systems. The main idea of IgA is to use the functions adopted in CAD systems not only to describe the domain geometry, but also to represent the numerical solution of the differential problem, within an isoparametric framework. Tensor-product B-splines and their rational extension, the so-called NURBS, are the dominant technology in CAD systems used in engineering, and thus also in IgA. One of the interesting features of IgA, compared to high order finite element methods, is that it allows for higher global regularity of the shape functions, up to C^{p-1} inter-element continuity for p-degree B-splines and NURBS. This leads to a higher accuracy per degree of freedom, as it has been shown in a wide class of problems and situations, ranging from solids and structures (see, e.g., [3–5]) to fluids (see, e.g., [6,7]). In addition, the high regularity of the shape functions also opened the door to geometrically flexible primal formulations for higher order PDEs (see, e.g., [8,9]).

The Galerkin formulation has been intensively employed in this context. However, the efficiency of the Galerkin method deeply depends on the numerical quadrature rules required in the construction of the corresponding linear systems. In contrast with the finite element context, where elementwise Gauss quadrature is known to be optimal, it is not yet completely understood how to construct efficient IgA quadrature rules, see, e.g., [10–12] and references therein.

The quadrature issue motivated the idea of taking advantage of IgA high regularity to construct efficient and geometrically flexible collocation methods, see [13] or the recent survey [14]. The major advantage of isogeometric collocation over Galerkin-type methods is the minimal computational effort with respect to quadrature, since for each degree of freedom only one point evaluation at a so-called collocation point is required. This property leads to extremely easy and fast constructions of the corresponding linear systems.

* Corresponding author at: Department of Civil Engineering and Architecture, University of Pavia, Italy.
E-mail addresses: manni@mat.uniroma2.it (C. Manni), alessandro.reali@unipv.it (A. Reali), speleers@mat.uniroma2.it (H. Speleers).

http://dx.doi.org/10.1016/j.camwa.2015.03.027
0898-1221/

In contrast with Galerkin-type formulations, collocation is based on the discretization of the strong form of the underlying PDE, which requires basis functions of sufficiently high order and smoothness. Consequently, the use of the IgA approach for collocation arises in a natural way, since spline functions (such as B-splines and NURBS) can be readily adjusted to any order of polynomial degree and continuity required by the differential operators at hand. It turns out that NURBS-based IgA collocation is very competitive with respect to Galerkin on the basis of an accuracy-to-computational-cost ratio, in particular when high degrees are adopted. For more details we refer the reader to the comprehensive study reported in [15].

Within the IgA collocation framework, several promising significant studies have been recently published, ranging from linear elastostatics and explicit dynamics [16] to phase-field modeling [17] and contact [18]. Moreover, IgA collocation has been successful in the context of structural elements: Bernoulli–Euler beam and Kirchhoff plate elements have been proposed in [19], while shear-deformable structural elements have been considered in a number of papers. In particular, mixed formulations both for Timoshenko initially-straight planar beams and for curved spatial rods have been proposed and studied in [20,21], respectively, while the extension to Reissner–Mindlin plate problems has been considered in [22]. A new single-parameter formulation for shear-deformable beams, recently introduced by [23], has been solved also via IgA collocation. Finally, robust and optimal solvers for the linear systems coming from the IgA collocation discretization have been proposed in [24].

Nonetheless, it is important to remark that the IgA paradigm is not confined to B-splines, NURBS and their localized extensions like T-splines [25–27], hierarchical splines [15,28–30] and LR-splines [31,32]. Other discretization spaces/techniques have also received some attention; for example, we can mention subdivision schemes [33], splines on triangulations [34–36] and generalized splines [37,38].

The so-called generalized B-splines (GB-splines) are piecewise functions with sections in more general spaces than algebraic polynomial spaces (like classical B-splines). Suitable selections of such spaces – typically including trigonometric or exponential functions – allow for an exact representation of polynomial curves, conic sections, helices and other profiles of salient interest in applications. In particular, conic sections are exactly parameterized by trigonometric/exponential generalized splines with respect to the arc length. GB-splines possess all fundamental properties of the classical (polynomial) B-splines; we highlight their recurrence relation, compact minimum support, local linear independence, and (non-stationary) subdivision rules. Moreover, contrarily to rational extensions like NURBS, they behave completely similar to B-splines with respect to differentiation and integration. For an overview of their properties we refer the reader to [38] and references therein. Finally, GB-splines support (locally refined) hierarchical structures in the same way as (polynomial) B-splines, see [39], and T-spline structures based on trigonometric generalized splines have been addressed in [40].

Tensor-product GB-splines and their hierarchical counterpart have been applied in IgA following the Galerkin formulation [37–39,41]. Thanks to their complete structural similarity with classical B-splines (which is based on a Bernstein-like representation), GB-splines are plug-to-plug compatible with B-splines in IgA. On the other hand, when dealing with GB-splines, the section spaces can be selected according to a problem-oriented strategy taking into account the geometrical and/or analytical peculiar issues of the specific addressed problem. The fine-tuning of the approximation spaces generally results in a gain from the accuracy point of view. These two aspects make GB-splines a flexible and interesting tool in IgA Galerkin approximation.

It is clear that IgA Galerkin methods based on GB-splines also suffer from the above mentioned quadrature issue, and a minimum number of point evaluations per degree of freedom is even more attractive in the context of GB-splines than for classical polynomial B-splines/NURBS. Moreover, GB-splines present the same smoothness properties and can be adjusted to any order (degree) as classical B-splines. Therefore, it is natural to consider IgA collocation methods based on GB-splines, and in this paper such a topic is addressed for the first time. Our aim is showing that discretization spaces consisting of suitable GB-splines are an excellent match for IgA collocation. In particular, we focus on collocation methods based on trigonometric and exponential generalized spline spaces for their relevance in practical applications.

The results of our investigation can be summarized as follows. Similarly to the Galerkin context, it turns out that isogeometric collocation methods based on generalized B-splines

- have a convergence behavior completely similar to isogeometric collocation methods based on polynomial B-splines;
- generally provide a gain from the accuracy point of view in comparison with polynomial B-splines and NURBS whenever the section spaces can be selected according to a problem-oriented strategy.

The remaining of the paper is divided into four sections. In the next section we briefly give the definition and the main properties of GB-splines of interest in the IgA collocation environment, with a special focus on trigonometric and exponential generalized B-splines. Section 3 introduces IgA collocation methods based on GB-splines in a simple 1D setting; it discusses the choice of the collocation points, and illustrates the performance of the presented approach in few numerical tests. Section 4 is devoted to the multivariate setting and addresses scalar- and vector-valued problems. In particular, IgA collocation methods based on GB-splines are described for advection–diffusion and linear elasticity problems, and they are numerically analyzed. Finally, Section 5 collects some concluding remarks.

2. Generalized B-splines

To make the paper self contained, this section is devoted to the definition and basic properties of GB-splines. Further details can be found in the cited references and, in particular, in [38, Section 3].

2.1. Non-polynomial spline spaces

Let Ξ be a sequence of knots over the interval $[0, 1]$,

$$\Xi := \{\xi_1 \le \xi_2 \le \cdots \le \xi_{m+p+1}\}, \quad m, p \in \mathbb{N}, \tag{1}$$

where we assume that the end points have a multiplicity $p + 1$, i.e.,

$$0 = \xi_1 = \cdots = \xi_{p+1} < \cdots < \xi_{m+1} = \cdots = \xi_{m+p+1} = 1. \tag{2}$$

Classical B-splines of degree p defined over (1) are a basis for piecewise polynomial functions with a suitable smoothness, i.e., functions with sections in the space of algebraic polynomials of degree p,

$$\mathbb{P}_p := \langle 1, t, \ldots, t^{p-2}, t^{p-1}, t^p \rangle.$$

Functions with a given smoothness and belonging piecewisely to more general spaces like

$$\mathbb{P}_p^{U_i,V_i} := \langle 1, t, \ldots, t^{p-2}, U_i(t), V_i(t) \rangle, \quad t \in [\xi_i, \xi_{i+1}),\ i = 1, \ldots, m + p, \tag{3}$$

can be considered as well, see [42] and references therein. In the section spaces (3) the functions U_i, V_i can be selected such that salient profiles of interest are exactly represented and/or special features are obtained. Popular choices for (3) are:

$$\mathbb{E}_{p,\alpha_i} := \langle 1, t, \ldots, t^{p-2}, \exp(\alpha_i t), \exp(-\alpha_i t) \rangle, \quad 0 < \alpha_i \in \mathbb{R}, \tag{4}$$

$$\mathbb{T}_{p,\alpha_i} := \langle 1, t, \ldots, t^{p-2}, \cos(\alpha_i t), \sin(\alpha_i t) \rangle, \quad 0 < \alpha_i(\xi_{i+1} - \xi_i) < \pi, \tag{5}$$

which lead to exponential and trigonometric splines, respectively. Exponential splines are often referred to as hyperbolic splines because the space (4) coincides with the space

$$\langle 1, t, \ldots, t^{p-2}, \cosh(\alpha_i t), \sinh(\alpha_i t) \rangle.$$

This alternative formulation shows more clearly the connection between the spaces (4) and (5).

Exponential and trigonometric splines allow for an exact representation of conic sections as well as some transcendental curves (helix, cycloid, ...). They are very attractive from the geometrical point of view. Indeed, in contrast with NURBS, they are able to provide parameterizations of conic sections with respect to the arc length so that equally spaced points in the parameter domain correspond to equally spaced points on the described curve.

For fixed values of the involved parameters, the spaces (4) and (5) have the same approximation power as $\mathbb{P}_p$, see [42, Section 3].

2.2. GB-splines: definition and properties

It is well known that it is possible to construct B-spline-like functions with sections in spaces as in (3), see [38,43,44] and references therein. The so-called *generalized B-splines (GB-splines) of degree p*, defined over the knot sequence (1), will be denoted by $\widehat{N}_{i,\Xi}^{(p)}$. To simplify the notation we omit the reference to the section spaces (3), even though this would be more appropriate. More precisely, we assume that

$$U_i, V_i \in C^{p-1}[\xi_i, \xi_{i+1}],$$

and that any non-trivial element in $\langle U_i^{(p-1)}, V_i^{(p-1)} \rangle$ has at most one zero in $[\xi_i, \xi_{i+1}]$. Thus, without loss of generality we may assume that

$$U_i^{(p-1)}(\xi_i) > 0,\ U_i^{(p-1)}(\xi_{i+1}) = 0, \qquad V_i^{(p-1)}(\xi_i) = 0,\ V_i^{(p-1)}(\xi_{i+1}) > 0.$$

GB-splines can then be defined by means of the following recurrence relation:

$$\widehat{N}_{i,\Xi}^{(1)}(t) := \begin{cases} \dfrac{V_i^{(p-1)}(t)}{V_i^{(p-1)}(\xi_{i+1})}, & \text{if } t \in [\xi_i, \xi_{i+1}), \\ \dfrac{U_{i+1}^{(p-1)}(t)}{U_{i+1}^{(p-1)}(\xi_{i+1})}, & \text{if } t \in [\xi_{i+1}, \xi_{i+2}), \\ 0, & \text{elsewhere,} \end{cases}$$

and

$$\widehat{N}_{i,\Xi}^{(p)}(t) := \delta_{i,\Xi}^{(p-1)} \int_{-\infty}^{t} \widehat{N}_{i,\Xi}^{(p-1)}(s)\mathrm{d}s - \delta_{i+1,\Xi}^{(p-1)} \int_{-\infty}^{t} \widehat{N}_{i+1,\Xi}^{(p-1)}(s)\mathrm{d}s, \quad p \ge 2,$$

where

$$\delta_{i,\Xi}^{(p)} := \frac{1}{\int_{-\infty}^{+\infty} \widehat{N}_{i,\Xi}^{(p)}(s)\mathrm{d}s},$$

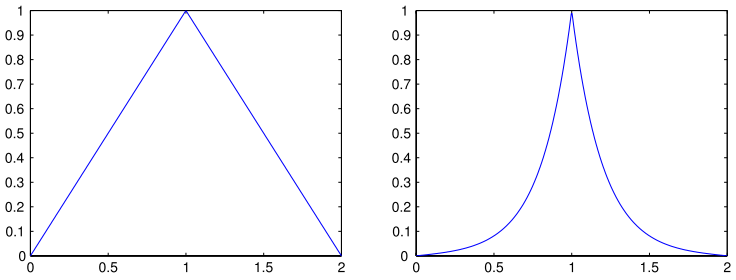

Fig. 1. GB-spline $\widehat{N}_{i,\Xi}^{(1)}$ with knot sequence $\Xi = \{0, 1, 2\}$. Left: The classical polynomial case. Right: The exponential case with $\alpha_i = 5$.

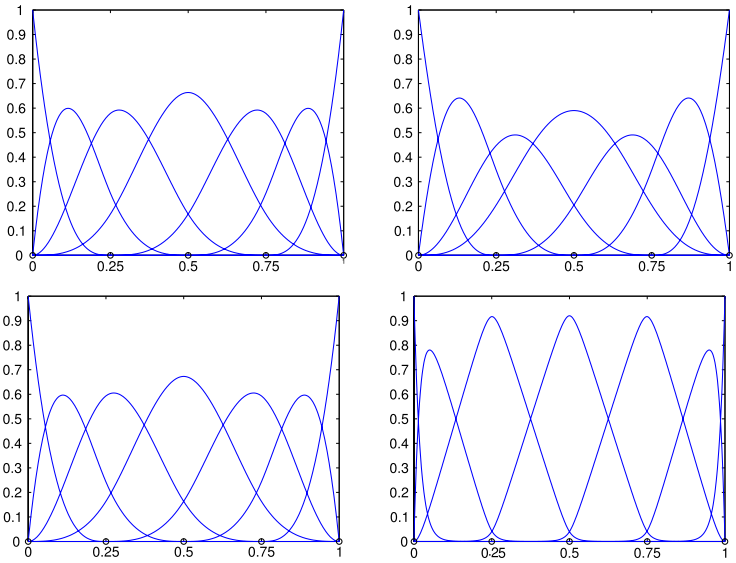

Fig. 2. Examples of GB-splines of degree 3 defined on the knot sequence $\Xi = \{0, 0, 0, 0, 1/4, 1/2, 3/4, 1, 1, 1, 1\}$. Top: Trigonometric B-splines with $\alpha_i = \frac{2}{3}\pi$ (left) and $\alpha_i = 3\pi$ (right). Bottom: Exponential B-splines with $\alpha_i = 3$ (left) and $\alpha_i = 50$ (right).

and fractions with zero denominators are considered to be zero. The knot sequence (1) allows us to define m GB-splines of degree p, namely $\widehat{N}_{1,\Xi}^{(p)}, \ldots, \widehat{N}_{m,\Xi}^{(p)}$. Two GB-splines of degree 1 are depicted in Fig. 1, and some sets of cubic generalized B-splines are illustrated in Fig. 2.

Generalized B-splines possess all desirable properties of classical polynomial B-splines [43,45]. We collect them in the following proposition.

Proposition 1. *Let $\widehat{N}_{i,\Xi}^{(p)}$, $i = 1, \ldots, m$, be generalized B-splines of degree $p \geq 2$ associated with the knot sequence (1). Then, the following properties hold:*

- *piecewise structure:* $\widehat{N}_{i,\Xi}^{(p)}(t) \in \mathbb{P}_p^{U_j,V_j}$, $t \in [\xi_j, \xi_{j+1})$;
- *positivity:* $\widehat{N}_{i,\Xi}^{(p)}(t) \geq 0$;
- *partition of unity:* $\sum_{i=1}^{m} \widehat{N}_{i,\Xi}^{(p)}(t) \equiv 1$, $t \in [\xi_{p+1}, \xi_{m+1})$;
- *compact support:* $\widehat{N}_{i,\Xi}^{(p)}(t) = 0$, $t \notin [\xi_i, \xi_{i+p+1}]$;
- *smoothness:* $\widehat{N}_{i,\Xi}^{(p)}(t)$ *is* $p - \rho_j$ *times continuously differentiable at* ξ_j *being* ρ_j *the multiplicity of* ξ_j *in the knot sequence;*
- *local linear independence:* $\widehat{N}_{i-p,\Xi}^{(p)}(t), \ldots, \widehat{N}_{i-1,\Xi}^{(p)}(t), \widehat{N}_{i,\Xi}^{(p)}(t)$ *are linearly independent on* $[\xi_i, \xi_{i+1})$.

In addition, a knot insertion procedure is also available, see [44], and the spaces (3) support a degree-raising process. Therefore, refinement strategies of common use in IgA based on NURBS (h, p, and k-refinement [2]) can be easily extended to IgA based on GB-splines.

In what follows we assume that, for $p \geq 3$, each internal knot has at most multiplicity ρ_j, with

$$\rho_j \leq p - 2, \quad j = p + 2, \ldots, m. \tag{6}$$

Therefore, the corresponding GB-splines are at least C^2 continuous in

$$(\xi_{p+1}, \xi_{m+1}) = (0, 1),$$

as required for the discretization of a second-order differential problem in strong form via a collocation approach. In the case $p = 2$, we assume that each internal knot has multiplicity 1 and $U_i, V_i \in C^p[\xi_i, \xi_{i+1}]$, so that the corresponding GB-splines are C^1 continuous in $(\xi_{p+1}, \xi_{m+1}) = (0, 1)$ but of class C^2 in (ξ_i, ξ_{i+1}). Similarly to the polynomial case with $p = 2$, such a configuration ensures a sufficient smoothness of the basis functions because the collocation points will be selected in the interior of the knot intervals (see later).

The space spanned by a fixed set of GB-splines will be referred to as *generalized spline space* and denoted by $\mathbb{GS}^p_\Xi$, i.e.,

$$\mathbb{GS}^p_\Xi := \langle \widehat{N}^{(p)}_{i,\Xi},\ i = 1, \ldots, m \rangle.$$

For a given degree p and a fixed knot sequence Ξ, GB-splines with section spaces as in (4) and (5) will be referred to as *exponential* and *trigonometric B-splines of degree p*, respectively. We will denote by

$$\mathbb{ES}^p_{\Xi,\boldsymbol{\alpha}},\ \mathbb{TS}^p_{\Xi,\boldsymbol{\alpha}},\ \mathbb{S}^p_\Xi$$

the spaces spanned by exponential, trigonometric and classical (polynomial) B-splines of degree p, respectively. Here $\boldsymbol{\alpha} = \{\ldots, \alpha_i, \ldots\}$ stands for the set of real parameters in (4) and (5). The spaces $\mathbb{ES}^p_{\Xi,\boldsymbol{\alpha}}$, $\mathbb{TS}^p_{\Xi,\boldsymbol{\alpha}}$ are called *exponential* and *trigonometric spline spaces*, respectively. For notational convenience we will denote by

$$\{N^{(p)}_{i,\Xi,\mathbb{E}},\ i = 1, \ldots, m\}, \qquad \{N^{(p)}_{i,\Xi,\mathbb{T}},\ i = 1, \ldots, m\}, \qquad \{N^{(p)}_{i,\Xi},\ i = 1, \ldots, m\}$$

the corresponding (generalized) B-spline bases.

It is interesting to notice that

$$\frac{\mathrm{d}}{\mathrm{d}t}\langle 1, t, \ldots, t^{p-2}, \exp(\alpha_i t), \exp(-\alpha_i t)\rangle = \langle 1, t, \ldots, t^{p-3}, \exp(\alpha_i t), \exp(-\alpha_i t)\rangle,$$
$$\frac{\mathrm{d}}{\mathrm{d}t}\langle 1, t, \ldots, t^{p-2}, \cos(\alpha_i t), \sin(\alpha_i t)\rangle = \langle 1, t, \ldots, t^{p-3}, \cos(\alpha_i t), \sin(\alpha_i t)\rangle,$$

so the differential operator acts on trigonometric and exponential splines in the same way as on classical polynomial splines. Hence, by taking into account (6) we have

$$\frac{\mathrm{d}}{\mathrm{d}t}\mathbb{ES}^p_{\Xi,\boldsymbol{\alpha}} = \mathbb{ES}^{p-1}_{\Xi,\boldsymbol{\alpha}}, \qquad \frac{\mathrm{d}}{\mathrm{d}t}\mathbb{TS}^p_{\Xi,\boldsymbol{\alpha}} = \mathbb{TS}^{p-1}_{\Xi,\boldsymbol{\alpha}}, \qquad \frac{\mathrm{d}}{\mathrm{d}t}\mathbb{S}^p_{\Xi,\boldsymbol{\alpha}} = \mathbb{S}^{p-1}_{\Xi,\boldsymbol{\alpha}}, \quad p \geq 2. \tag{7}$$

NURBS do not possess a property like (7). This property makes the structural similarity between exponential, trigonometric and polynomial splines even stronger.

Exponential and trigonometric B-splines approach polynomial B-splines as the parameters α_i tend to zero. The same is true if, for fixed values of α_i, the length of the intervals $\xi_{i+1} - \xi_i$ tends to zero.

The section spaces in (3) may be different on each interval. Thus, GB-splines allow for an exact representation of profiles composed by a sequence of curve segments of different kind: Arcs of ellipses, hyperbolas, polynomial curves, etc.

Multivariate versions of the above spaces can be obtained straightforwardly by the usual tensor-product approach. Of course, univariate spaces of different kind can be considered in the different directions.

3. IgA collocation in 1D

In this section, following the presentation of [13], we introduce the basic ideas of IgA collocation in a very simple 1D setting. The presentation is general and any approximation space guaranteeing the minimum required regularity can be used in principle. However, we herein focus only on GB-splines. In this framework, we discuss three different possible choices of collocation points. We then conclude the section presenting some numerical tests.

3.1. Formulation

Let f, β, γ be real functions in $C^0[a, b]$, with $a < b$ given real numbers. Let $g_0, g_1 \in \mathbb{R}$ be scalars and $\mathcal{BC}_0$, $\mathcal{BC}_1 : C^1[a, b] \to \mathbb{R}$ be linear operators. The following simple 1D model problem is considered: Find a real function $u \in C^2[a, b]$ such that

$$\begin{cases} -u''(x) + \beta(x)u'(x) + \gamma(x)u(x) = f(x), & \forall x \in (a, b), \\ \mathcal{BC}_i(u) = g_i, & i = 0, 1, \end{cases} \tag{8}$$

where u', u'' represent the first and second derivatives of u, respectively. We assume that (8) has one and only one solution u, and that the boundary condition operators $\mathcal{BC}_i$ are linearly independent on $\mathbb{P}_1$, i.e., on the space of linear functions.

We now want to discretize the problem in (8) via IgA collocation. Given $n \in \mathbb{N}$, let $\mathcal{V}^M \subset C^2[a, b]$ be a spline space (which could be, e.g., a space of GB-splines or NURBS) of dimension $M := n+2$ on the interval $[a, b]$. Given $n+2$ collocation points in $[a, b]$, $a = \tau_1 < \tau_2 < \cdots < \tau_{n+2} = b$, we obtain the following discrete problem: Find $u_M \in \mathcal{V}^M$ such that

$$\begin{cases} -u_M''(\tau_j) + \beta(\tau_j)u_M'(\tau_j) + \gamma(\tau_j)u_M(\tau_j) = f(\tau_j), & j = 2, \ldots, n+1, \\ \mathcal{B}C_i(u_M) = g_i, & i = 0, 1. \end{cases} \tag{9}$$

In this work we consider $\mathcal{V}^M \subset C^2[a, b]$ to be a proper GB-spline space $\mathbb{GS}^p_\Xi$ of dimension $M = n + 2$.[1]

3.2. Collocation points and theoretical results

The discrete problem (9) is defined once a strategy for the selection of the collocation points is set. Such a selection is of paramount importance, because it directly influences the stability and convergence properties of the collocation scheme. In this section we summarize the main results concerning the selection of the collocation points in NURBS-based IgA, and then we briefly discuss the choice of the collocation points in the generalized B-spline context.

3.2.1. Collocation points in the NURBS context

In NURBS-based IgA collocation literature, (the images of)[2] the so-called Greville abscissae have been widely adopted as the default choice, given their simple definition and good results from a practical point of view in virtually every situation. The Greville abscissae corresponding to the space $\mathbb{S}^p_\Xi$, $p \geq 1$, are defined from the knot vector Ξ in (1) as averages of consecutive knots, namely [45]

$$\xi^{(p)}_{i,*} := \frac{\xi_{i+1} + \cdots + \xi_{i+p}}{p}, \quad i = 1, \ldots, m. \tag{10}$$

They are well known in the CAD and approximation literature for a number of properties. In particular, they typically give a stable interpolation, except in some cases where high degrees are combined with particular non-uniform meshes. On the other hand, the so-called Demko abscissae are instead proven to be always stable [46]. The (images of the) second derivative Demko abscissae have been proven to be the best choice as collocation points [13]. Nevertheless, they are not used in practice because they do not possess a simple explicit expression but they have to be computed by an iterative algorithm.

The selection of points guaranteeing a stable interpolation is a fundamental issue for a collocation scheme, since it is proven in [13] that this implies optimal convergence (i.e., of order $p - 1$) in the $W^{2,\infty}$-norm (or, equivalently, in the H^2-norm). Such a proof is valid only in 1D and cannot be extended to higher dimensions. However, extensive numerical testing has shown that the convergence rates obtained in 1D are attained also in higher dimensions.

Moreover, optimal convergence rates are not recovered in the L^∞- and $W^{1,\infty}$-norms (or, equivalently, in the L^2- and H^1-norms), where it has been numerically shown that, in the context of NURBS-based IgA collocation, orders of convergence p and $p - 1$ for even and odd degrees, respectively, are attained. We remark that, despite not being optimal in the L^2- and H^1-norms, the obtained orders of convergence are increasing with p, and the cost of collocation is much lower than that of Galerkin approaches of the same order, especially as p increases. This makes IgA collocation very competitive with respect to Galerkin on the basis of an accuracy-to-computational-cost ratio, in particular when higher degrees (e.g., $p > 3$) are adopted. For more details we refer the reader to the comprehensive study reported in [15].

3.2.2. Collocation points in the GB-spline context

Moving from NURBS-based IgA collocation results to the framework of GB-splines, we consider three sets of points as possible candidates to be collocation sites, namely standard B-spline Greville, GB-spline Greville, and GB-spline Demko abscissae. The two latter choices are discussed in the following.

We first recall that the Greville abscissae corresponding to $\mathbb{S}^p_\Xi$, $p \geq 1$, are determined as the coefficients of the identity function when expressed in terms of the B-spline basis $\{N^{(p)}_{i,\Xi},\ i = 1, \ldots, m\}$ on the interval $[\xi_{p+1}, \xi_{m+1})$. From this, relation (10) is easily derived [45].

Greville abscissae can be also defined in generalized spline spaces as the coefficients of the identity function t represented in the GB-spline basis $\{\widehat{N}^{(p)}_{i,\Xi},\ i = 1, \ldots, m\}$ on the interval $[\xi_{p+1}, \xi_{m+1})$. From (3) it follows that, in general, $t \in \mathbb{GS}^p_\Xi$ on the interval $[\xi_{p+1}, \xi_{m+1})$ only if $p \geq 3$. Therefore, it makes sense to look for Greville abscissae in the space of generalized splines only if $p \geq 3$. The expression of the Greville abscissae related to cubic generalized B-splines (i.e., $p = 3$) with general section spaces can be found in [47, Section 3]. More precisely, they are given by the values of the first component of the vector in

[1] In some numerical tests we will also consider quadratic spaces ($p = 2$), namely $\mathbb{GS}^2_\Xi$. The elements in these spaces are not C^2 but possess a sufficient smoothness at the collocation points whenever the collocation points are selected in the interior of each knot interval, see Section 2.

[2] The general IgA approach involves a geometry map $\mathbf{G}$ (see Section 4), and we are referring to the image through this map. In the 1D setting, however, the geometry map is not so crucial, so we postpone some details to the multivariate setting.

Eq. (22) in the mentioned paper. For trigonometric and exponential B-splines defined on the (extended) equally spaced knots

$$\begin{aligned} &\xi_1 = \cdots = \xi_{p+1} < \xi_{p+2} < \cdots < \xi_m < \xi_{m+1} = \cdots = \xi_{m+p+1}, \\ &\xi_{k+1} := \xi_k + h, \qquad k = p+1, \ldots, m, \end{aligned} \tag{11}$$

with $p = 3$, the above mentioned formulas can be simplified as follows. For the cubic trigonometric spline space $\mathbb{TS}^3_{\Xi,\boldsymbol{\alpha}}$ with $\alpha_i = \alpha$ and knots as in (11), the corresponding Greville abscissae are

$$\begin{aligned} &\xi^{(3)}_{1,*,\mathbb{T}} := \xi_4, \\ &\xi^{(3)}_{2,*,\mathbb{T}} := \xi_4 + \frac{h\alpha - \sin(h\alpha)}{h\alpha(1-\cos(h\alpha))}h, \\ &\xi^{(3)}_{k,*,\mathbb{T}} := \xi_{k+2}, \quad k = 3, \ldots, m-2, \\ &\xi^{(3)}_{m-1,*,\mathbb{T}} := \xi_{m+1} - \frac{h\alpha - \sin(h\alpha)}{h\alpha(1-\cos(h\alpha))}h, \\ &\xi^{(3)}_{m,*,\mathbb{T}} := \xi_{m+1}. \end{aligned} \tag{12}$$

For the cubic exponential spline space $\mathbb{ES}^3_{\Xi,\boldsymbol{\alpha}}$ with $\alpha_i = \alpha$ and knots as in (11), the corresponding Greville abscissae are

$$\begin{aligned} &\xi^{(3)}_{1,*,\mathbb{E}} := \xi_4, \\ &\xi^{(3)}_{2,*,\mathbb{E}} := \xi_4 + \frac{h\alpha - \sinh(h\alpha)}{h\alpha(1-\cosh(h\alpha))}h, \\ &\xi^{(3)}_{k,*,\mathbb{E}} := \xi_{k+2}, \quad k = 3, \ldots, m-2, \\ &\xi^{(3)}_{m-1,*,\mathbb{E}} := \xi_{m+1} - \frac{h\alpha - \sinh(h\alpha)}{h\alpha(1-\cosh(h\alpha))}h, \\ &\xi^{(3)}_{m,*,\mathbb{E}} := \xi_{m+1}. \end{aligned} \tag{13}$$

Explicit expressions for the Greville abscissae related to exponential or trigonometric spline spaces of higher degree can be computed as well. However, as mentioned in Section 2.2, it follows that they approach (10) when the meshsize tends to zero. Therefore, the Greville abscissae related to (polynomial) B-splines can be also used as collocation points for exponential or trigonometric splines of the same degree whenever sufficiently fine grids are considered.

Let us now focus on the Demko abscissae. We recall from [13] that the only collocation choice in the B-spline case which is proven to be stable for any mesh and degree is the one proposed by Demko [46]. The so-called Demko abscissae are the points where the Chebyshev spline attains its extrema. The Chebyshev spline is the (polynomial) spline with the maximum number of oscillations, for which the extrema take the values ± 1 (see, e.g., [45, Chapter XIII]). Demko abscissae can be also defined for generalized spline spaces in the same way, and for their computation one can use a similar iterative algorithm as the one proposed for B-splines in [45, Chapter XIII]. The arguments used in [13] to prove the stability of the collocation method can be easily extended from the B-spline to the GB-spline context. If we consider the trigonometric spline space $\mathbb{TS}^p_{\Xi,\boldsymbol{\alpha}}$ or the exponential spline space $\mathbb{ES}^p_{\Xi,\boldsymbol{\alpha}}$ as discretization space to solve problem (9), then we obtain a stable set of collocation points by taking the Demko points related to the space $\mathbb{TS}^{p-2}_{\Xi,\boldsymbol{\alpha}}$ or $\mathbb{ES}^{p-2}_{\Xi,\boldsymbol{\alpha}}$ of second derivatives of $\mathbb{TS}^p_{\Xi,\boldsymbol{\alpha}}$ or $\mathbb{ES}^p_{\Xi,\boldsymbol{\alpha}}$, respectively (see (7)).

In Fig. 3 we illustrate different choices of point sets in the GB-spline context. In particular, for the GB-spline bases given in Fig. 2, we show the corresponding Greville abscissae ($\triangle$) and the Demko abscissae ($\triangledown$). For comparison purposes, we also depict the standard B-spline Greville abscissae ($\diamond$). We see that the different sets of points behave very similarly. The B-spline Greville abscissae are the easiest to compute, whereas the GB-spline Demko abscissae have the highest computational cost. Finally, the Chebyshev splines in the corresponding GB-spline spaces are shown in Fig. 4.

3.3. Numerical results

We now present some numerical experiments in 1D where we employ IgA collocation methods based on trigonometric B-splines of different degrees. Our aim is to verify the performance of the methods in terms of convergence rates and compare the behavior of the three sets of collocation points presented in the previous section, i.e., standard B-spline Greville, GB-spline Greville, and GB-spline second-derivative Demko abscissae.[3]

[3] Following [13], in our 1D numerical tests we have not included results for $p = 2$, since this case is not covered by the theory presented in that paper. Moreover, we note that $p = 2$ could be chosen only in the case of standard B-spline Greville abscissae, while, in the other cases, $p \geq 3$ is indeed needed (see the discussion in Section 3.2.2). On the other hand, in the 2D numerical tests presented in the following section, where we choose to collocate at standard B-spline Greville abscissae, we show results for $p \geq 2$.

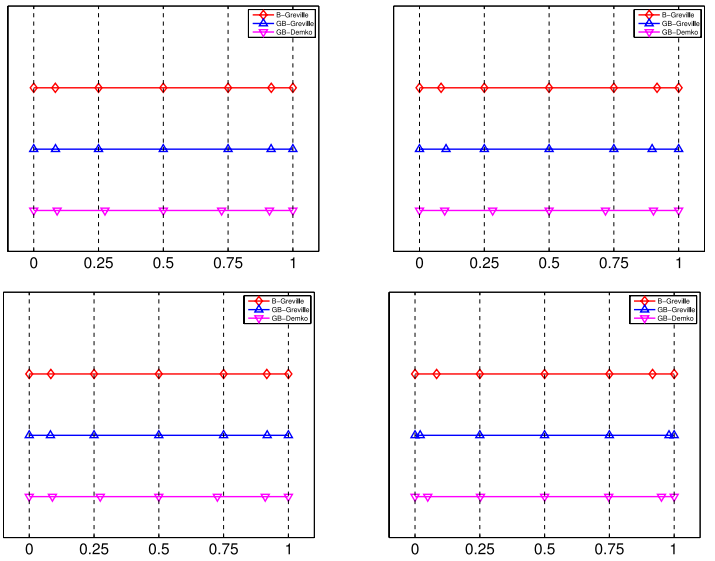

Fig. 3. Examples of sets of collocation points related to GB-splines of degree 3 defined on the knot sequence $\Xi = \{0, 0, 0, 0, 1/4, 1/2, 3/4, 1, 1, 1, 1\}$. We compare the B-spline Greville abscissae, the GB-spline Greville abscissae, and the GB-spline Demko abscissae. Top: Trigonometric B-splines with $\alpha_i = \frac{2}{3}\pi$ (left) and $\alpha_i = 3\pi$ (right). Bottom: Exponential B-splines with $\alpha_i = 3$ (left) and $\alpha_i = 50$ (right).

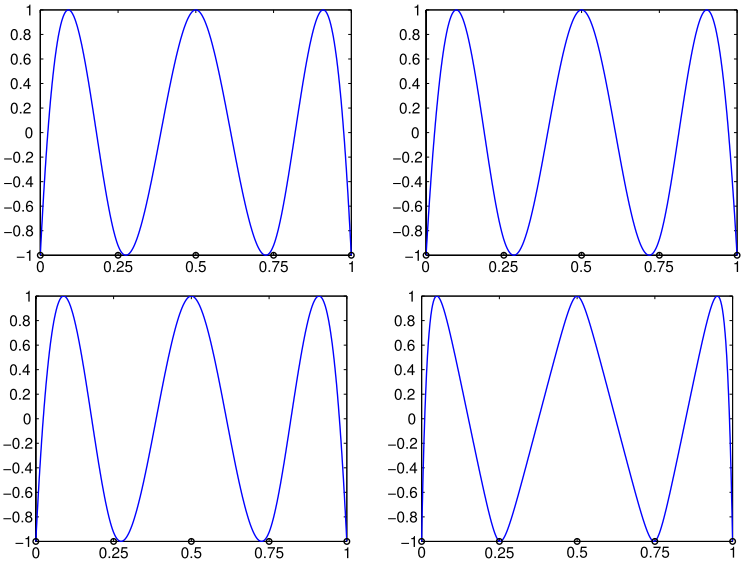

Fig. 4. Chebyshev splines related to GB-spline spaces of degree 3 defined on the knot sequence $\Xi = \{0, 0, 0, 0, 1/4, 1/2, 3/4, 1, 1, 1, 1\}$. Top: Trigonometric splines with $\alpha_i = \frac{2}{3}\pi$ (left) and $\alpha_i = 3\pi$ (right). Bottom: Exponential splines with $\alpha_i = 3$ (left) and $\alpha_i = 50$ (right).

3.3.1. 1D model problem

We consider the following model problem defined on $[0, 1]$:

$$\begin{cases} -u'' + u' + u = (1 + 4\pi^2)\sin(2\pi x) - 2\pi\cos(2\pi x), & \forall x \in (0, 1), \\ u(0) = u(1) = 0, \end{cases} \tag{14}$$

with exact solution:

$$u(x) = \sin(2\pi x). \tag{15}$$

This problem is numerically solved using the collocation method outlined in the previous sections in the space $\mathbb{TS}^p_{\Xi,\boldsymbol{\alpha}}$ of trigonometric splines with $\alpha_i = 3\pi$ and knots as in (11), for different degrees and different choices of the collocation points. In Fig. 5, we report log-scale plots of the relative errors, for the different sets of collocation points, in both L^∞- and $W^{1,\infty}$-norms. The obtained results show that – just like with NURBS-based IgA collocation – in both norms, an order of convergence p is attained for even degrees, while an order $p - 1$ is attained for odd degrees.

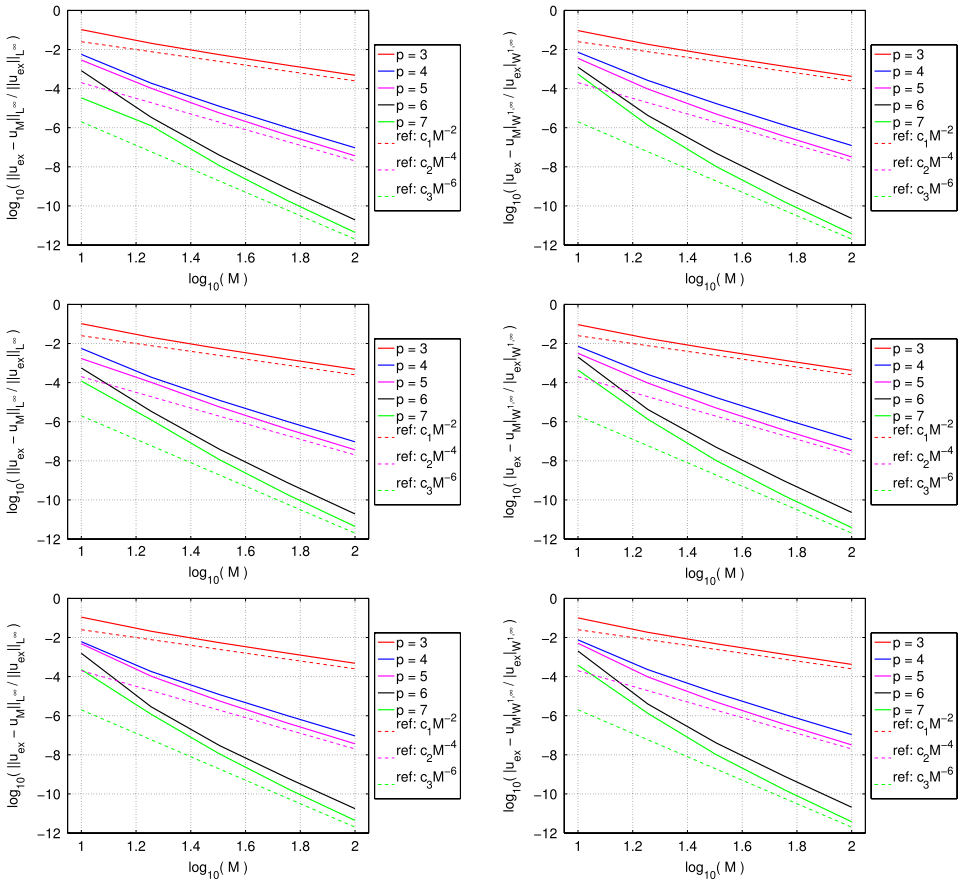

Fig. 5. 1D model problem. Relative error in L^∞-norm (left) and $W^{1,\infty}$-norm (right) using trigonometric B-splines with $\alpha_i = 3\pi$ and $p = 3, \ldots, 7$. Top: Collocation at standard B-spline Greville abscissae. Middle: Collocation at GB-spline Greville abscissae. Bottom: Collocation at GB-spline second-derivative Demko abscissae.

In the $W^{2,\infty}$-norm (see Fig. 6), instead, we observe the expected optimal order of convergence, i.e., $p-1$, for all considered approximation degrees in agreement with the theoretical predictions of [13].

3.3.2. 1D eigenvalue problem

A remarkable result of Galerkin-based IgA is its capability of approximating higher modes, without introducing spurious "optical branches" in the numerical spectrum (see, e.g., [48–51]). The same feature is present also in IgA collocation, as it has been shown in [13] in the context of NURBS-based approximations. We want to show that this feature also occurs in the case of GB-splines. To this end, we consider the following 1D eigenvalue problem:

$$\begin{cases} u'' + \omega^2 u = 0, \quad \forall x \in (0,1), \\ u(0) = u(1) = 0, \end{cases} \tag{16}$$

for which the exact frequencies ω_l are given by

$$\omega_l = \pi l, \quad \text{with } l = 1, 2, 3, \ldots \tag{17}$$

The problem in (16) is solved using IgA collocation in the space of trigonometric B-splines with knots as in (11) and considering standard B-spline Greville abscissae as collocation points. In Fig. 7, we report the results in terms of normalized discrete spectra in the space $\mathbb{TS}^p_{\Xi,\boldsymbol{\alpha}}$ with $\alpha_i = 3\pi$, obtained by considering a linear parameterization and using different degrees of approximation (we have used $n = 1000$, see Section 3.1, to produce each spectrum). We clearly observe the good behavior of all spectra, which converge for an increasing degree. Similarly to IgA Galerkin/collocation based on polynomial B-splines, few "outlier frequencies" can be seen at the end of the spectrum. For more details on this and other aspects of spectrum analysis via IgA Galerkin or collocation methods, the reader is referred to [13,48–51].

Since we are using a quite fine discretization (the length of any knot span is about 10^{-3}), trigonometric B-splines with $\alpha_i = 3\pi$ basically behave like classical polynomial B-splines (see Section 2.2). This is in a perfect agreement with the numerical results shown in Fig. 7, which are completely analogous to those obtained in the polynomial B-spline case (see [13, Figure 14] for a comparison).

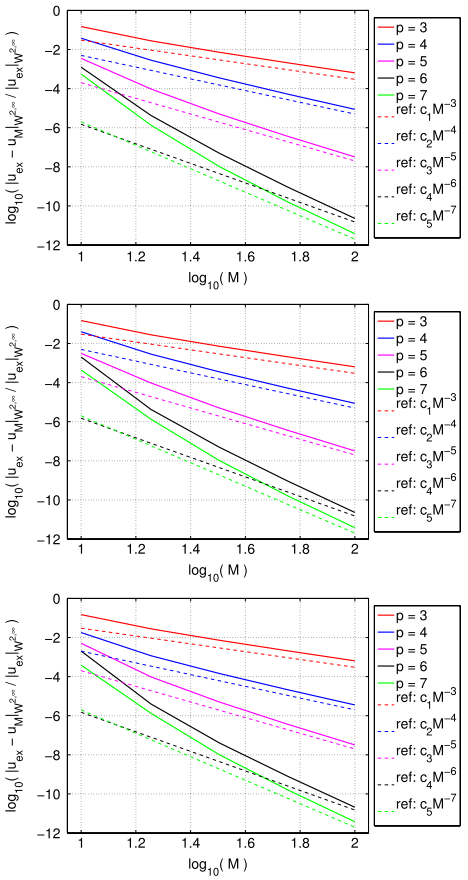

Fig. 6. 1D model problem. Relative error in $W^{2,\infty}$-norm using trigonometric B-splines with $\alpha_i = 3\pi$ and $p = 3, \ldots, 7$. Top: Collocation at standard B-spline Greville abscissae. Middle: Collocation at GB-spline Greville abscissae. Bottom: Collocation at GB-spline second-derivative Demko abscissae.

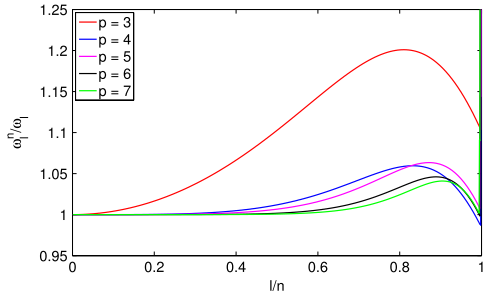

Fig. 7. 1D eigenvalue problem. Normalized spectra using trigonometric B-splines with $\alpha_i = 3\pi$ and $p = 3, \ldots, 7$. Collocation is performed at standard B-spline Greville abscissae.

On the other hand, an improvement of the normalized discrete spectra can be obtained by using high frequency values for $\boldsymbol{\alpha}$ in the approximating trigonometric space $\mathbb{TS}^p_{\Xi,\boldsymbol{\alpha}}$, mainly for large degrees. In Fig. 8 we compare, for $p = 7, \ldots, 10$, the normalized discrete spectra obtained by using polynomial splines with those provided by trigonometric splines with parameters α_i selected according to the following heuristic rule:

$$\alpha_i = \frac{p}{p+4}\pi n. \tag{18}$$

Again, we have used $n = 1000$ to produce each spectrum. We observe that the gain obtained by using high frequency section spaces is twofold. First, a larger subset of the exact spectrum is approximated in a very good way. Second, the peak of the error in the approximation is reduced, while the number of outliers remains the same. This can be roughly explained by the fact that when considering trigonometric splines with very high frequencies there is a better match between the approximation and the real solution of the problem, exactly in those regions (high frequencies) where classical polynomial B-splines present less appealing performance.

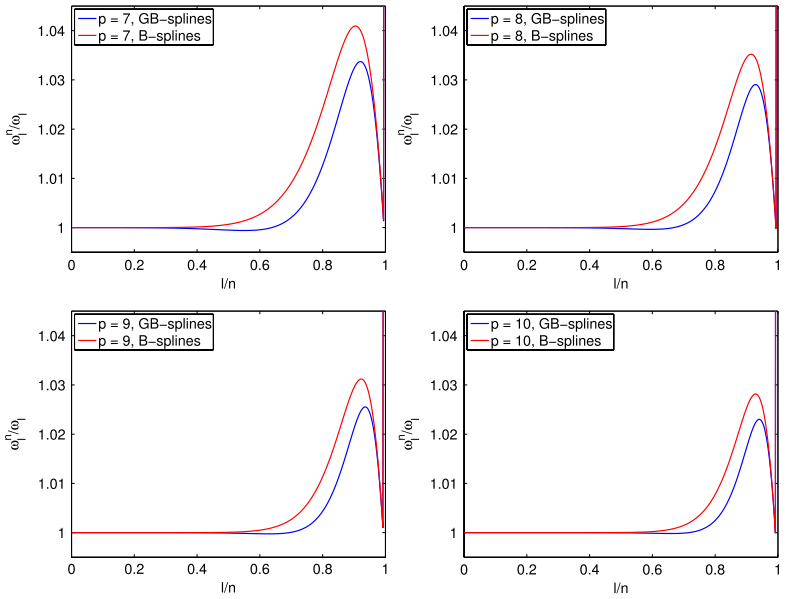

Fig. 8. 1D eigenvalue problem. Normalized spectra using polynomial B-splines (red) and trigonometric B-splines (blue) with α_i selected according to (18). Top: $p = 7$ (left) and $p = 8$ (right); bottom: $p = 9$ (left) and $p = 10$ (right). Collocation is performed at standard B-spline Greville abscissae.

We finally remark that, when collocation is performed at GB-spline Greville or Demko abscissae, completely similar spectral results are obtained. The corresponding plots are not reported here for the sake of brevity.

4. IgA collocation for multi-dimensional scalar- and vector-valued problems

In this section, we extend the previously introduced IgA collocation methods to the multi-dimensional case, considering first advection–diffusion as a scalar-valued model problem, and then resorting to linear elasticity as a vector-valued model problem. Accordingly, in the following, we present the basic equations of both model problems and we approximate them via IgA collocation methods. In both cases, we implement IgA collocation using GB-splines and standard Greville abscissae, and we solve some numerical examples in 2D showing the good overall behavior, as well as some clear advantages, of GB-splines in the context of IgA collocation.

4.1. IgA collocation for advection–diffusion: formulation

Let us consider the following advection–diffusion problem defined on a domain $\Omega \subset \mathbb{R}^d$:

$$-\nabla \cdot (\kappa \nabla u) + \boldsymbol{\beta} \cdot \nabla u = f, \quad \text{in } \Omega, \tag{19}$$

complemented by the Dirichlet boundary conditions

$$u = g_D, \quad \text{on } \Gamma_D, \tag{20}$$

and by the Neumann boundary conditions

$$\kappa \nabla u \cdot \mathbf{n} = g_N, \quad \text{on } \Gamma_N. \tag{21}$$

In the equations above, $u(\mathbf{x})$ is the unknown field ($\mathbf{x}$ being the position vector), ∇ is the standard nabla operator, $\Gamma = \Gamma_D \bigcup \Gamma_N$ is the boundary of the domain, with $\Gamma_D \bigcap \Gamma_N = \emptyset$, and $\mathbf{n}$ is the unit outward normal to Γ. Moreover, κ and $\boldsymbol{\beta}$ are a scalar and a vector parameter function, respectively. Finally, suitable regularity requirements are assumed to hold for f, g_D, and g_N.

Isogeometric collocation emanates from the combination of the isogeometric technology and the classical collocation method. More precisely, let

$$\{\hat{\varphi}_1, \ldots, \hat{\varphi}_M\} \tag{22}$$

be a set of basis functions defined on $\widehat{\Omega} := [0, 1]^d$, such that the physical domain Ω in (19) can be described by a global geometry function,

$$\mathbf{G} : \widehat{\Omega} \to \overline{\Omega}, \qquad \mathbf{G}(\mathbf{t}) := \sum_{i=1}^{M} \hat{\varphi}_i(\mathbf{t})\, \boldsymbol{c}_i, \quad \boldsymbol{c}_i \in \mathbb{R}^d, \ \mathbf{t} \in \widehat{\Omega}. \tag{23}$$

We assume that the map $\mathbf{G}$ is invertible in $\widehat{\Omega}$ and $\mathbf{G}(\partial\widehat{\Omega}) = \partial\overline{\Omega}$.

Following the isoparametric approach, we consider the approximation space $\mathcal{V}^M$ spanned by

$$\varphi_i(\mathbf{x}) := \hat{\varphi}_i(\mathbf{G}^{-1}(\mathbf{x})) = \hat{\varphi}_i(\mathbf{t}), \quad i = 1, \ldots, M, \ \mathbf{x} = \mathbf{G}(\mathbf{t}). \tag{24}$$

In the original formulation of IgA the functions $\hat{\varphi}_i$ in (24) are chosen to be tensor-product NURBS. Here, we consider as discretization spaces the tensor-product generalized spline spaces described in Section 2. Therefore, we seek an approximation u_M to the unknown exact solution field u of the advection–diffusion problem in the form

$$u_M = \sum_{i=1}^{M} \boldsymbol{\varphi}_i(\mathbf{x})\bar{u}_i = \sum_{i=1}^{M} \hat{\boldsymbol{\varphi}}_i\left(\mathbf{G}^{-1}(\mathbf{x})\right)\bar{u}_i, \tag{25}$$

where $\hat{\varphi}_i$, $i = 1, \ldots, M$, are tensor-product GB-splines and $\bar{u}_1, \ldots, \bar{u}_M$ are the unknown coefficients. Expression (25) has to be substituted into Eqs. (19)–(21).

Let us assume that $d = 2$. We denote by m_1 and m_2 the number of degrees of freedom in the two parametric directions, so that $M := m_1 m_2$ is the total number of degrees of freedom. Thus, M scalar equations are needed to determine the unknown coefficients. We choose M collocation points $\boldsymbol{\tau}_{kl}$, $k = \{1, \ldots, m_1\}$, $l = \{1, \ldots, m_2\}$ given by

$$\boldsymbol{\tau}_{kl} := \mathbf{G}(\hat{\boldsymbol{\tau}}_{kl}), \tag{26}$$

where $\hat{\boldsymbol{\tau}}_{kl}$ are a set of M collocation points in the parametric domain $\widehat{\Omega}$; for example, tensor-products of B-spline Greville abscissae in both directions as defined in (10). The collocation points for $k = 1, m_1$ and $l = 1, m_2$ are assumed to be located at the boundary Γ. Separate sets of equations are taken for the patch interior and for the boundaries.

In the patch interior Ω, we obtain $(m_1 - 2)(m_2 - 2)$ scalar equations by collocating equation (32) at the points $\boldsymbol{\tau}_{kl}$, $k = \{2, \ldots, m_1 - 1\}$, $l = \{2, \ldots, m_2 - 1\}$:

$$\left[-\nabla \cdot (\kappa \nabla u_M) + \boldsymbol{\beta} \cdot \nabla u_M - f\right](\tau_{kl}) = 0, \quad \boldsymbol{\tau}_{kl} \in \Omega. \tag{27}$$

At the Dirichlet boundary Γ_D we impose

$$u_M(\boldsymbol{\tau}_{kl}) = g_D(\boldsymbol{\tau}_{kl}), \quad \boldsymbol{\tau}_{kl} \in \Gamma_D. \tag{28}$$

Thanks to the properties of the (G)B-splines associated with the knot sequence (2), the above equations can be separated from the rest of the resulting linear system.[4]

To enforce Neumann boundary conditions, Eq. (21) is collocated at the points $\boldsymbol{\tau}_{kl} \in \Gamma_N$. A distinction is necessary between the collocation points located at the edges ($k = 1, m_1$ and $l = 2, \ldots, m_2 - 1$, or $l = 1, m_2$ and $k = 2, \ldots, m_1 - 1$), and those located at the corners of the domain ($k = 1, m_1$ and $l = 1, m_2$). For collocation points located on edges within the Neumann boundary, the equations are

$$\left[\kappa \nabla u_M \cdot \mathbf{n} - g_N\right](\boldsymbol{\tau}_{kl}) = 0, \quad \tau_{kl} \in \text{edge} \subset \Gamma_N. \tag{29}$$

Instead, for collocation points located at corners where two Neumann boundaries meet, it has been proven in [16] (in the context of elasticity) that the appropriate equations are

$$\left[\kappa \nabla u_M \cdot \mathbf{n}^L - g_N^L\right](\boldsymbol{\tau}_{kl}) + \left[\kappa \nabla u_M \cdot \mathbf{n}^R - g_N^R\right](\boldsymbol{\tau}_{kl}) = 0, \quad \boldsymbol{\tau}_{kl} \equiv \text{corner} \subset \Gamma_N, \tag{30}$$

where $\mathbf{n}^L$ and $\mathbf{n}^R$ are the unit outward normals of the edges meeting at the corner, and g_N^L and g_N^R are the respective values of the Neumann boundary conditions.

4.2. IgA collocation for advection–diffusion: numerical results

To numerically test the formulation described above, we consider two advection–diffusion problems, one featuring a manufactured smooth solution over a mapped geometry, and the other presenting sharp boundary layers. The first example aims at showing that the convergence rates observed in 1D are attained also in higher dimensions, as it was presented in the context of B-splines and NURBS in previous works on IgA collocation (see, e.g., [13,15,16]). The second example aims at showing that, as we stressed in the introduction, GB-splines can provide a gain from the accuracy point of view in comparison with polynomial B-splines and NURBS whenever the section spaces can be selected according to a problem-oriented strategy.

[4] The coefficients in (25) not determined by (28) will be referred to as the "internal coefficients" and the corresponding number of degrees of freedom as the "internal degrees of freedom". We wish to highlight that, like in the case of Galerkin-based IgA, Dirichlet boundary conditions can be strongly enforced exactly, only when g_D can be exactly represented in terms of the shape functions (i.e., GB-splines here). Fortunately, this happens to be the case in many engineering applications, where constant or linear Dirichlet conditions are typically enforced. We also remark that, for homogeneous Dirichlet boundary conditions, isogeometric elements have double zeros at the domain corners.

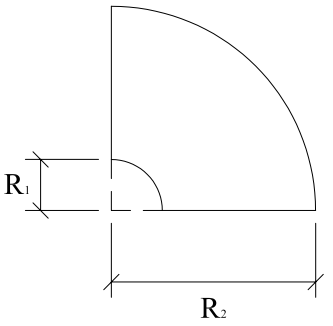

Fig. 9. Problem domain: Quarter of an annulus.

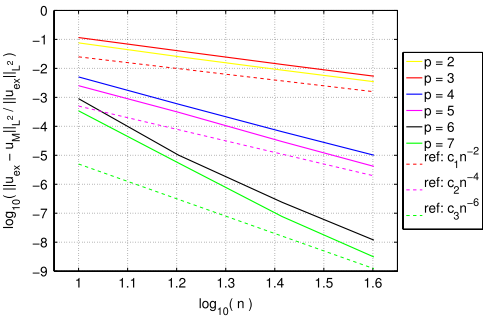

Fig. 10. Advection–diffusion on a quarter of an annulus. Relative errors in L^2-norm versus the square root of the number of degrees of freedom $n = \sqrt{M}$ for different degrees. Collocation is performed at standard tensor-product B-spline Greville abscissae, using a tensor-product of polynomial B-splines and trigonometric B-splines with $\alpha_i = \pi/2$ and $p = q = 2, \ldots, 7$.

4.2.1. IgA collocation for an advection–diffusion problem on a quarter of an annulus

In this example we consider a 2D domain constituted by a quarter of an annulus, as sketched in Fig. 9, with internal and external radii equal to $R_1 = 1$ and $R_2 = 4$, respectively. The domain can be exactly represented by a single tensor-product spline patch, using a polynomial spline of degree $p \geq 1$ in one parametric direction and a trigonometric spline of degree $q \geq 2$ with $\alpha_i = \pi/2$ in the other parametric direction. The whole domain boundary is assumed to be subjected to homogeneous Dirichlet boundary conditions, and we assign a manufactured solution, namely

$$u(x, y) = e^x xy(x^2 + y^2 - 1)(x^2 + y^2 - 16). \tag{31}$$

Such a manufactured solution satisfies the prescribed boundary conditions, and the right-hand side f is computed from it using Eq. (19). The parameters are assumed to be $\kappa = 1$ and $\boldsymbol{\beta} = [1,\ 1]^T$.

The problem is solved by IgA collocation using, within a classical isoparametric framework, a tensor-product of polynomial B-splines of degree p and trigonometric B-splines of degree q, with $\alpha_i = \pi/2$ and equally spaced knots as in (11). Standard tensor-product B-spline Greville abscissae are considered as collocation points. In Fig. 10 we present the results for degrees $p = q = 2, \ldots, 7$ in terms of relative errors of u in the L^2-norm versus the square root of the total number of degrees of freedom $n = \sqrt{M}$. It can be seen that the convergence rates already observed in the 1D case (i.e., p and $p - 1$ for even and odd degree p, respectively) are attained.

4.2.2. IgA collocation for an advection–diffusion problem on the unit square with boundary layers

As a second test we consider a 2D advection–diffusion problem described in [10]. We consider problem (19) where the parameters are assumed to be $\kappa = 10^{-3}$ and $\boldsymbol{\beta} = [1,\ 0]^T$, while the right-hand side has a constant value $f = 1$. Homogeneous Dirichlet boundary conditions are applied to the entire boundary of the problem domain, which is the unit square $[0, 1]^2$. The exact solution of such a problem is a ramp of unit slope along the x-axis, showing two layers at $y = 0$ and $y = 1$, and a third, sharper layer at $x = 1$.

This problem is solved by IgA collocation considering both tensor-product polynomial B-splines and tensor-product exponential B-splines. In both cases we use standard tensor-product B-spline Greville abscissae as collocation points and we consider a uniform knot distribution as in (11). For the exponential B-splines we choose the parameter α_i to be equal to the global Péclet number, i.e., $\alpha_i = \mathrm{Pe}_g = \|\boldsymbol{\beta}\|/\kappa = 10^3$. In Figs. 11 and 12 we present some results for degrees $p = q = 4$ and different choices of uniform knot distributions. We can see that, as expected, classical (polynomial) B-splines lead to spurious oscillations until the discretization is fine enough to resolve the boundary layers. A discretization consisting of 300×300 internal degrees of freedom (i.e., 302×302 in total) is needed to get a solution where the oscillations (indeed still

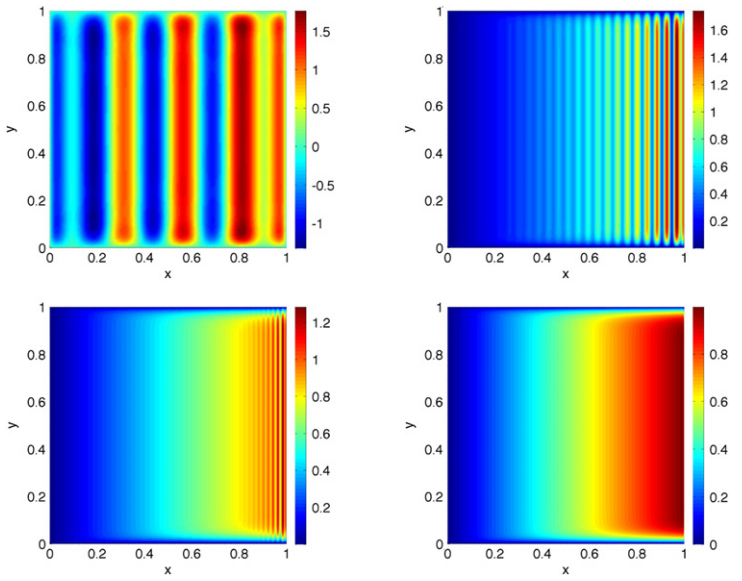

Fig. 11. Advection–diffusion on the unit square. Contour plots of the numerical solution field u_M. Collocation is performed at standard tensor-product B-spline Greville abscissae, using $p = q = 4$ and standard tensor-product B-splines (top, left: 10×10 internal degrees of freedom; top, right: 50×50; bottom, left: 100×100; bottom, right: 300×300).

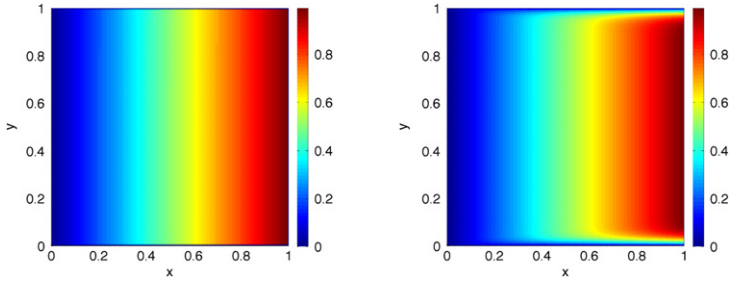

Fig. 12. Advection–diffusion on the unit square. Contour plots of the numerical solution field u_M. Collocation is performed at standard tensor-product B-spline Greville abscissae, using $p = q = 4$ and tensor-product exponential B-splines with $\alpha_i = \mathrm{Pe}_g = \|\boldsymbol{\beta}\|/\kappa = 10^3$ (left: 10×10 internal degrees of freedom; right: 50×50).

present) are negligible in the "eyeball norm". Instead, with exponential B-splines and the adopted selection of the parameter α_i, already a very coarse discretization (with 10×10 internal degrees of freedom) leads to acceptable results. However, we notice that in this case the two boundary layers at $y = 0$ and $y = 1$ appear to be too sharp, as compared with the behavior of the B-spline case with 300×300 internal degrees of freedom. A less coarse discretization (with 50×50 internal degrees of freedom) gives a solution that, in practice, cannot be distinguished from the 300×300 B-spline case. Moreover, we remark that, in contrast with the 300×300 B-spline discretization, no oscillations (not even very small) are observed in this case.

4.3. IgA collocation for linear elasticity: formulation

Let now $\Omega \subset \mathbb{R}^d$ represent an elastic body subjected to body forces $\mathbf{f}$, to prescribed displacements $\mathbf{g}_D$ on a portion of the boundary Γ_D, and to (possibly zero) prescribed tractions $\mathbf{g}_N$ on the remaining portion Γ_N, being $\Gamma = \Gamma_D \bigcup \Gamma_N$ the boundary of the domain, with $\Gamma_D \bigcap \Gamma_N = \emptyset$. Suitable regularity requirements are assumed to hold for $\mathbf{f}$, $\mathbf{g}_D$, and $\mathbf{g}_N$.

The small-strain linear elastostatic problem in strong form is then defined as

$$-\nabla \cdot \left(\mathbb{C}\nabla^S \mathbf{u}\right) = \mathbf{f}, \quad \text{in } \Omega, \tag{32}$$

complemented by the Dirichlet boundary conditions

$$\mathbf{u} = \mathbf{g}_D, \quad \text{on } \Gamma_D, \tag{33}$$

and by the Neumann boundary conditions

$$\left(\mathbb{C}\nabla^S \mathbf{u}\right) \cdot \mathbf{n} = \mathbf{g}_N, \quad \text{on } \Gamma_N, \tag{34}$$

where $\mathbf{u}(\mathbf{x})$ is the unknown displacement field ($\mathbf{x}$ being the position vector), ∇^S is the symmetric part of the standard nabla operator, $\mathbb{C}$ is the fourth-order elasticity tensor, and $\mathbf{n}$ is the unit outward normal to the boundary of the domain.

The construction of the IgA collocation method is completely analogous to the one described in Section 4.1, in the context of scalar-valued problems. Using the isoparametric approach, we seek an approximation $\mathbf{u}_M$ to the unknown exact solution field $\mathbf{u}$ of the elastic problem in the form

$$\mathbf{u}_M = \sum_{i=1}^{M} \hat{\varphi}_i \left(\mathbf{G}^{-1}(\mathbf{x})\right) \bar{\mathbf{u}}_i, \tag{35}$$

where $\hat{\varphi}_i$, $i = 1, \ldots, M$, are the tensor-product GB-splines which, following the isoparametric paradigm, are also used to represent the geometry of the problem. The unknown vectors $\bar{\mathbf{u}}_i \in \mathbb{R}^d$ will be referred to as displacement coefficients. Then, expression (35) has to be substituted into Eqs. (32)–(34).

Let us assume that $d = 2$. We denote by m_1 and m_2 the number of basis functions in the two parametric directions. Then $M = m_1 m_2$ is the total number of unknown coefficients per displacement component. Analogously to Section 4.1, we choose M collocation points $\boldsymbol{\tau}_{kl}$, $k = \{1, \ldots, m_1\}$, $l = \{1, \ldots, m_2\}$ located at the images of the tensor-product Greville abscissae of the knot vectors. In this case, $2M$ scalar equations are needed to determine the displacement coefficients.

In the patch interior Ω, we obtain $2\,(m_1 - 2)\,(m_2 - 2)$ scalar equations by collocating equation (32) at the points $\boldsymbol{\tau}_{kl}$, $k = \{2, \ldots, m_1 - 1\}$, $l = \{2, \ldots, m_2 - 1\}$:

$$\left[\nabla \cdot \left(\mathbb{C}\nabla^S \mathbf{u}_M\right) + \mathbf{f}\right](\boldsymbol{\tau}_{kl}) = \mathbf{0}, \quad \boldsymbol{\tau}_{kl} \in \Omega. \tag{36}$$

The Dirichlet and the Neumann boundaries are treated as in the scalar-valued case. In particular, to enforce Neumann boundary conditions, equation (34) is collocated at the points $\boldsymbol{\tau}_{kl} \in \Gamma_N$ according to the following strategy, see [16]:

$$\left[\left(\mathbb{C}\nabla^S \mathbf{u}_M\right) \cdot \mathbf{n} - \mathbf{g}_N\right](\boldsymbol{\tau}_{kl}) = \mathbf{0}, \quad \boldsymbol{\tau}_{kl} \in \text{edge} \subset \Gamma_N. \tag{37}$$

$$\left[\left(\mathbb{C}\nabla^S \mathbf{u}_M\right) \cdot \mathbf{n}^L - \mathbf{g}_N^L\right](\boldsymbol{\tau}_{kl}) + \left[\left(\mathbb{C}\nabla^S \mathbf{u}_M\right) \cdot \mathbf{n}^R - \mathbf{g}_N^R\right](\boldsymbol{\tau}_{kl}) = \mathbf{0}, \quad \boldsymbol{\tau}_{kl} \equiv \text{corner} \subset \Gamma_N, \tag{38}$$

where, again, $\mathbf{n}^L$ and $\mathbf{n}^R$ are the unit outward normals of the edges meeting at the corner, and $\mathbf{g}_N^L$ and $\mathbf{g}_N^R$ are the respective imposed tractions. In addition, we refer the reader to [16] for a detailed discussion on the conditions to be imposed in more complicate situations like at the interfaces of multi-patch geometries.

We highlight that, as it has been shown in [18], the above approach to impose Neumann boundary conditions may lead to spurious oscillations in situations implying solutions of reduced regularity, when non-uniform meshes are adopted. In such cases, alternative methods for imposing Neumann boundary conditions should be considered, and in the same paper two simple strategies to cure this have been presented.

4.4. IgA collocation for linear elasticity: numerical results

To numerically test the formulation above, we consider a plane strain problem, defined on the same quarter of an annulus as described in Section 4.2.1 and sketched in Fig. 9. The whole domain boundary is assumed to be clamped (i.e., homogeneous Dirichlet boundary conditions are considered) and we assign the following manufactured solution in terms of displacement components

$$u(x, y) = v(x, y) = \mathrm{e}^x xy(x^2 + y^2 - 1)(x^2 + y^2 - 16). \tag{39}$$

The manufactured solution satisfies the prescribed boundary conditions, and the load is computed from it by imposing equilibrium.

The problem is solved by IgA collocation based on a tensor-product of polynomial B-splines of degree p and trigonometric B-splines of degree q, with $\alpha_i = \pi/2$ and uniform knots as in (11). Standard tensor-product B-spline Greville abscissae are taken as collocation points. Fig. 13 depicts the results for degrees $p = q = 2, \ldots, 7$ in terms of the relative errors of the first component of the displacement and of one component (σ_{11}) of the stress in the L^2-norm versus the square root of the total number of control points $n = \sqrt{M}$. Similar convergence behaviors are obtained also for the other components. It can be seen that, also here, the convergence rates already observed in the 1D case (Section 3.3) and in the advection–diffusion case (Section 4.2) are attained.

5. Conclusions

We have introduced isogeometric collocation methods based on GB-splines and we have analyzed their performance through numerical examples for univariate and multivariate scalar- and vector-valued problems. In particular, we have focused on isogeometric collocation methods based on trigonometric and exponential generalized spline spaces because of their relevance in practical applications.

As already pointed out for the isogeometric Galerkin approach, GB-splines can be a useful tool in isogeometric collocation methods due to the following three main reasons:

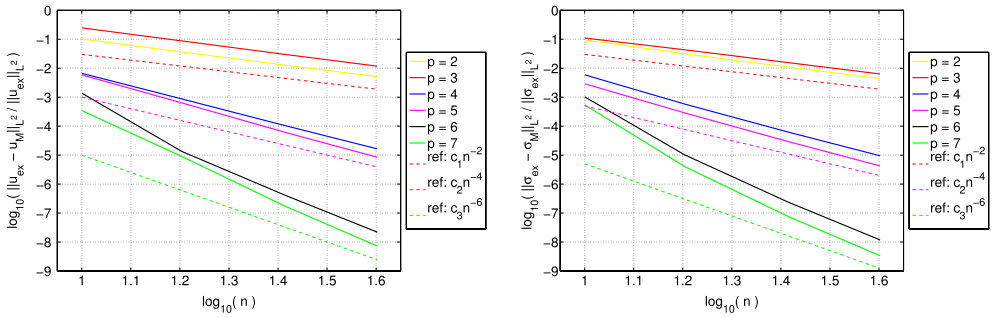

Fig. 13. Plane strain clamped quarter of an annulus. Error plots for the first component of the displacement (left) and for the stress σ_{11} (right) versus $n = \sqrt{M}$, i.e., the square root of the total number of displacement coefficients. Collocation is performed at standard tensor-product B-spline Greville abscissae, using a tensor-product of polynomial B-splines and trigonometric B-splines with $\alpha_i = \pi/2$ and $p = q = 2, \ldots, 7$.

- GB-splines allow for exact and optimal (i.e., with respect to the arc length) parameterizations of geometries of salient interest in applications. This deeply and positively affects the behavior of the geometry map constructed according to the isoparametric approach.
- Section spaces of GB-splines can be selected according to a problem-oriented strategy. For example, exponential generalized B-splines can be profitably used whenever the solution presents particular features like sharp layers.
- GB-splines have a structure which is completely similar to classical (polynomial) B-splines: This makes generalized B-splines and (polynomial) B-splines plug-to-plug compatible from the implementation point of view.

According to the performed numerical experiments, IgA collocation methods based on trigonometric and exponential B-splines show a convergence behavior similar to classical (polynomial) B-splines and NURBS whenever the section spaces are selected without a specific relation with the problem to be solved. On the other hand, a gain from the accuracy point of view is generally achieved whenever the section spaces can be selected according to a problem-oriented strategy, taking into account the geometrical and/or analytical peculiar issues of the specific addressed problem. We finally highlight that in this paper we focused only on single-patch geometries; however, extensions to conforming multi-patch geometries can be easily implemented following [16]. Extensions to more complex situations, involving, e.g., non-conforming multiple patches and/or trimming surfaces is a topic still to be addressed in the isogeometric collocation literature, and will be the topic of future research in the context of both classical and generalized B-splines.

Acknowledgments

This work was partially supported by the MIUR 'Futuro in Ricerca' Programme through the projects "DREAMS" and "Isogeometric Discretizations in Continuum Mechanics", as well as by the European Research Council through the FP7 Ideas Starting Grant no. 259229 "ISOBIO". Finally, the authors would like to thank Prof. Tom Hughes (University of Texas at Austin) for the very valuable discussions on the subject of this paper.

References

[1] T.J.R. Hughes, J.A. Cottrell, Y. Bazilevs, Isogeometric analysis: CAD, finite elements, NURBS, exact geometry, and mesh refinement, Comput. Methods Appl. Mech. Engrg. 194 (2005) 4135–4195.
[2] J.A. Cottrell, T.J.R. Hughes, Y. Bazilevs, Isogeometric Analysis: Toward Integration of CAD and FEA, John Wiley & Sons, 2009.
[3] J.F. Caseiro, R.A.F. Valente, A. Reali, J. Kiendl, F. Auricchio, R.J. Alves de Sousa, Assumed natural strain NURBS-based solid-shell element for the analysis of large deformation elasto-plastic thin-shell structures, Comput. Methods Appl. Mech. Engrg. 284 (2015) 861–880.
[4] T. Elguedj, Y. Bazilevs, V.M. Calo, T.J.R. Hughes, $\bar{B}$ and $\bar{F}$ projection methods for nearly incompressible linear and non-linear elasticity and plasticity using higher-order NURBS elements, Comput. Methods Appl. Mech. Engrg. 197 (2008) 2732–2762.
[5] S. Morganti, F. Auricchio, D.J. Benson, F.I. Gambarin, S. Hartmann, T.J.R. Hughes, A. Reali, Patient-specific isogeometric structural analysis of aortic valve closure, Comput. Methods Appl. Mech. Engrg. 284 (2015) 508–520.
[6] Y. Bazilevs, V.M. Calo, J.A. Cottrell, T.J.R. Hughes, A. Reali, G. Scovazzi, Variational multiscale residual-based turbulence modeling for large eddy simulation of incompressible flows, Comput. Methods Appl. Mech. Engrg. 197 (2007) 173–201.
[7] Y. Bazilevs, C. Michler, V.M. Calo, T.J.R. Hughes, Isogeometric variational multiscale modeling of wall-bounded turbulent flows with weakly enforced boundary conditions on unstretched meshes, Comput. Methods Appl. Mech. Engrg. 199 (2010) 780–790.
[8] H. Gomez, V.M. Calo, Y. Bazilevs, T.J.R. Hughes, Isogeometric analysis of the Cahn–Hilliard phase-field model, Comput. Methods Appl. Mech. Engrg. 197 (2008) 4333–4352.
[9] J. Kiendl, K.-U. Bletzinger, J. Linhard, R. Wüchner, Isogeometric shell analysis with Kirchhoff–Love elements, Comput. Methods Appl. Mech. Engrg. 198 (2009) 3902–3914.
[10] F. Auricchio, F. Calabrò, T.J.R. Hughes, A. Reali, G. Sangalli, A simple algorithm for obtaining nearly optimal quadrature rules for NURBS-based isogeometric analysis, Comput. Methods Appl. Mech. Engrg. 249–252 (2012) 15–27.
[11] T.J.R. Hughes, A. Reali, G. Sangalli, Efficient quadrature for NURBS-based isogeometric analysis, Comput. Methods Appl. Mech. Engrg. 199 (2010) 301–313.
[12] D. Schillinger, S. Hossain, T. Hughes, Reduced Bézier element quadrature rules for quadratic and cubic splines in isogeometric analysis, Comput. Methods Appl. Mech. Engrg. 277 (2014) 1–45.
[13] F. Auricchio, L. Beirão da Veiga, T.J.R. Hughes, A. Reali, G. Sangalli, Isogeometic collocation methods, Math. Models Methods Appl. Sci. 20 (2010) 2075–2107.

[14] A. Reali, T.J.R. Hughes, An introduction to isogeometric collocation methods, in: G. Beer, S.P. Bordas (Eds.), Isogeometric Methods for Numerical Simulation, Springer, 2015, ICES Report 14-30.
[15] D. Schillinger, J.A. Evans, A. Reali, M.A. Scott, T.J.R. Hughes, Isogeometric collocation: cost comparison with Galerkin methods and extension to adaptive hierarchical NURBS discretizations, Comput. Methods Appl. Mech. Engrg. 267 (2013) 170–232.
[16] F. Auricchio, L. Beirão da Veiga, T.J.R. Hughes, A. Reali, G. Sangalli, Isogeometric collocation for elastostatics and explicit dynamics, Comput. Methods Appl. Mech. Engrg. 249–252 (2012) 2–14.
[17] H. Gomez, A. Reali, G. Sangalli, Accurate, efficient, and (iso)geometrically flexible collocation methods for phase-field models, J. Comput. Phys. 262 (2014) 153–171.
[18] L. De Lorenzis, J.A. Evans, A. Reali, T.J.R. Hughes, Isogeometric collocation: Neumann boundary conditions and contact, Comput. Methods Appl. Mech. Engrg. 284 (2015) 21–54.
[19] A. Reali, H. Gomez, An isogeometric collocation approach for Bernoulli–Euler beams and Kirchhoff plates, Comput. Methods Appl. Mech. Engrg. 284 (2015) 623–636.
[20] L. Beirão da Veiga, C. Lovadina, A. Reali, Avoiding shear locking for the Timoshenko beam problem via isogeometric collocation methods, Comput. Methods Appl. Mech. Engrg. 241–244 (2012) 38–51.
[21] F. Auricchio, L. Beirão da Veiga, J. Kiendl, C. Lovadina, A. Reali, Locking-free isogeometric collocation methods for spatial Timoshenko rods, Comput. Methods Appl. Mech. Engrg. 263 (2013) 113–126.
[22] J. Kiendl, F. Auricchio, L. Beirão da Veiga, C. Lovadina, A. Reali, Isogeometric collocation methods for the Reissner–Mindlin plate problem, Comput. Methods Appl. Mech. Engrg. 284 (2015) 489–507.
[23] J. Kiendl, F. Auricchio, T.J.R. Hughes, A. Reali, Single-variable formulations and isogeometric discretizations for shear deformable beams, Comput. Methods Appl. Mech. Engrg. 284 (2015) 988–1004.
[24] M. Donatelli, C. Garoni, C. Manni, S. Serra-Capizzano, H. Speleers, Robust and optimal multi-iterative techniques for IgA collocation linear systems, Comput. Methods Appl. Mech. Engrg. 284 (2015) 1120–1146.
[25] Y. Bazilevs, V.M. Calo, J.A. Cottrell, J.A. Evans, T.J.R. Hughes, S. Lipton, M.A. Scott, T.W. Sederberg, Isogeometric analysis using T-splines, Comput. Methods Appl. Mech. Engrg. 199 (2010) 229–263.
[26] L. Beirão da Veiga, A. Buffa, D. Cho, G. Sangalli, Analysis-suitable T-splines are dual-compatible, Comput. Methods Appl. Mech. Engrg. 249–252 (2012) 42–51.
[27] X. Li, M.A. Scott, Analysis-suitable T-splines: characterization, refineability, and approximation, Math. Models Methods Appl. Sci. 24 (2014) 1141–1164.
[28] C. Giannelli, B. Jüttler, H. Speleers, THB-splines: the truncated basis for hierarchical splines, Comput. Aided Geom. Design 29 (2012) 485–498.
[29] C. Giannelli, B. Jüttler, H. Speleers, Strongly stable bases for adaptively refined multilevel spline spaces, Adv. Comput. Math. 40 (2014) 459–490.
[30] A.-V. Vuong, C. Giannelli, B. Jüttler, B. Simeon, A hierarchical approach to adaptive local refinement in isogeometric analysis, Comput. Methods Appl. Mech. Engrg. 200 (2011) 3554–3567.
[31] T. Dokken, T. Lyche, K.F. Pettersen, Polynomial splines over locally refined box-partitions, Comput. Aided Geom. Design 30 (2013) 331–356.
[32] K.A. Johannessen, T. Kvamsdal, T. Dokken, Isogeometric analysis using LR B-splines, Comput. Methods Appl. Mech. Engrg. 269 (2014) 471–514.
[33] P.B. Bornemann, F. Cirak, A subdivision-based implementation of the hierarchical B-spline finite element method, Comput. Methods Appl. Mech. Engrg. 253 (2013) 584–598.
[34] N. Jaxon, X. Qian, Isogeometric analysis on triangulations, Comput. Aided Design 46 (2014) 45–57.
[35] H. Speleers, C. Manni, F. Pelosi, From NURBS to NURPS geometries, Comput. Methods Appl. Mech. Engrg. 255 (2013) 238–254.
[36] H. Speleers, C. Manni, F. Pelosi, M.L. Sampoli, Isogeometric analysis with Powell–Sabin splines for advection–diffusion–reaction problems, Comput. Methods Appl. Mech. Engrg. 221–222 (2012) 132–148.
[37] P. Costantini, C. Manni, F. Pelosi, M.L. Sampoli, Quasi-interpolation in isogeometric analysis based on generalized B-splines, Comput. Aided Geom. Design 27 (2010) 656–668.
[38] C. Manni, F. Pelosi, M.L. Sampoli, Generalized B-splines as a tool in isogeometric analysis, Comput. Methods Appl. Mech. Engrg. 200 (2011) 867–881.
[39] C. Manni, F. Pelosi, H. Speleers, Local hierarchical h-refinements in IgA based on generalized B-splines, in: M. Floater, et al. (Eds.), Mathematical Methods for Curves and Surfaces 2012, in: LNCS, vol. 8177, Springer-Verlag, 2014, pp. 341–363.
[40] C. Bracco, D. Berdinsky, D. Cho, M.-J. Oh, T.-W. Kim, Trigonometric generalized T-splines, Comput. Methods Appl. Mech. Engrg. 268 (2014) 540–556.
[41] C. Manni, F. Pelosi, M.L. Sampoli, Isogeometric analysis in advection–diffusion problems: tension splines approximation, J. Comput. Appl. Math. 236 (2011) 511–528.
[42] P. Costantini, T. Lyche, C. Manni, On a class of weak Tchebycheff systems, Numer. Math. 101 (2005) 333–354.
[43] B.I. Kvasov, P. Sattayatham, GB-splines of arbitrary order, J. Comput. Appl. Math. 104 (1999) 63–88.
[44] G. Wang, M. Fang, Unified and extended form of three types of splines, J. Comput. Appl. Math. 216 (2008) 498–508.
[45] C. de Boor, A Practical Guide to Splines, revised ed., Springer, 2001.
[46] S. Demko, On the existence of interpolation projectors onto spline spaces, J. Approx. Theory 43 (1985) 151–156.
[47] P. Costantini, C. Manni, Geometric construction of generalized cubic splines, Rend. Mat. Appl. 26 (2006) 327–338.
[48] J.A. Cottrell, A. Reali, Y. Bazilevs, T.J.R. Hughes, Isogeometric analysis of structural vibrations, Comput. Methods Appl. Mech. Engrg. 195 (2006) 5257–5296.
[49] T.J.R. Hughes, J.A. Evans, A. Reali, Finite element and NURBS approximations of eigenvalue, boundary-value, and initial-value problems, Comput. Methods Appl. Mech. Engrg. 271 (2014) 290–320.
[50] T.J.R. Hughes, A. Reali, G. Sangalli, Duality and unified analysis of discrete approximations in structural dynamics and wave propagation: comparison of p-method finite elements with k-method NURBS, Comput. Methods Appl. Mech. Engrg. 197 (2008) 4104–4124.
[51] A. Reali, An isogeometric analysis approach for the study of structural vibrations, J. Earthquake Eng. 10 (2006) 1–30.